nature communications

Article

https://doi.org/10.1038/s41467-024-52833-1

A selective frequency damping and Janus adhesive hydrogel as bioelectronic interfaces for clinical trials

Received: 2 May 2024

Accepted: 24 September 2024

Published online: 01 October 2024

Check for updates

Jiabei Luo[1,6], Yuefan Jin[2,6], Linpeng Li[2] ✉, Boya Chang[1], Bin Zhang[1], Kerui Li[1], Yaogang Li[3], Qinghong Zhang[3], Hongzhi Wang[1], Jing Wang[4,5], Shankai Yin[2], Hui Wang[2] ✉ & Chengyi Hou[1] ✉

Maintaining stillness is essential for accurate bioelectrical signal acquisition, but dynamic noise from breathing remains unavoidable. Isotropic adhesives are often used as bioelectronic interfaces to ensure signal fidelity, but they can leave irreversible residues, compromising device accuracy. We propose a hydrogel with selective frequency damping and asymmetric adhesion as a bioelectronic interface. This hydrogel mitigates dynamic noise from breathing, with a damping effect in the breathing frequency range 60 times greater than at other frequencies. It also exhibits an asymmetric adhesion difference of up to 537 times, preventing residues. By homogenizing ion distribution, extending Debye length, and densifying the electric field, the hydrogel ensures stable signal transmission over 10,000 cycles. Additionally, it can non-invasively diagnose otitis media with higher sensitivity than invasive probes and has been effective in clinical polysomnography monitoring, aiding in the diagnosis of obstructive sleep apnea.

Bioelectrical signals serve as valuable tools in clinical practice, offering insights into physiological functions, aiding diagnosis and treatment, and contributing to advancements in healthcare delivery and research[1–4]. In clinical practice, subjects typically need to remain stationary to obtain bioelectrical signals with improved spatiotemporal resolution and accuracy. However, in a stationary state, or even during sleep or anesthesia, subjects continue to breathe, and the dynamic noise produced by breathing can create signal artefacts that can compromise the target bioelectrical signals[5,6].

To selectively remove the dynamic noise embedded in these bioelectrical signals, processing techniques such as bandpass filtering are used[7]. However, these techniques may result in the loss of signal information, as well as suffer from signal delay after processing[8]. Therefore, the application of damping materials as bioelectronic interfaces to absorb dynamic noise in real-time and transmit bioelectrical signals is crucial in the context of bioelectrical signals. Park et al. presented a hydrogel damper based on phase transition, which exhibits a rubbery state for damping low-frequency noise and a glassy state for transmitting high-frequency signals[9]. Nonetheless, in order to meet the demand for high bioelectrical sensitivity, it is necessary to make hydrogel dampers adhesive to improve skin compliance and thus avoid the creation of voids[10]. This will result in a lowering of the interfacial impedance and an improvement in the quality of the signal transmission[11].

Hydrogels can achieve reliable adhesion to the target biological target through strategies such as mechanical interlocking, diffusion

[1]State Key Laboratory for Modification of Chemical Fibers and Polymer Materials, College of Materials Science and Engineering, Donghua University, Shanghai, P. R. China. [2]Shanghai Key Laboratory of Sleep Disordered Breathing, Department of Orolaryngology-Head and Neck Surgery, Otolaryngology Institute of Shanghai Jiao Tong University, Shanghai Sixth People's Hospital Affiliated to Shanghai Jiao Tong University School of Medicine, Shanghai, P. R. China. [3]Engineering Research Center of Advanced Glasses Manufacturing Technology, Ministry of Education, Donghua University, Shanghai, P. R. China. [4]Institute of Environmental Engineering, ETH Zürich, Zürich, Switzerland. [5]Laboratory for Advanced Analytical Technologies, Empa – Swiss Federal Laboratories for Materials Science and Technology, Dübendorf, Switzerland. [6]These authors contributed equally: Jiabei Luo, Yuefan Jin.
✉e-mail: lilp@sjtu.edu.cn; wangh2005@alumni.sjtu.edu.cn; hcy@dhu.edu.cn

theory, and chemical bonding[12,13]. For this reason, adhesive hydrogels have been applied as bioelectronic interfaces, and further enable high spatiotemporal resolution and high-fidelity bioelectric signal transmissions[14–16]. However, current adhesive hydrogels used for bioelectronic interfaces exhibit isotropic adhesion, which can cause undesired residues that affect device accuracy after multiple uses[17].

Janus adhesive hydrogel is an effective solution for addressing the issue of undesired residues. Its asymmetric structure provides asymmetric adhesion, allowing it to exhibit varying degrees of adhesion on different surfaces[18]. Wang et al. proposed a Janus adhesive hydrogel by controlling the interfacial distribution of free carboxyl groups on the two sides of the hydrogels and used it to address postoperative adhesion problems[19]. Similarly, Xu et al. proposed a Janus adhesive hydrogel with nanoparticles at one side induced by the magnetic field and applied it for wearable human motion sensing and enhanced low-grade heat harvesting[20]. However, the currently available Janus adhesive hydrogels have neither been able to achieve reliable bioelectrical signal transmission nor possess the ability to selectively remove dynamic noise.

Hence, in order to effectively utilize Janus adhesive hydrogels for selectively removing dynamic noise in the context of bioelectrical signals, it is essential to tackle the following challenges: (1) achieving the balance between asymmetric adhesion and maintaining consistent overall damping; (2) preventing the distortion of bioelectrical signal transmission caused by asymmetric structural features; and (3) reconciling the conflict between the need for weak bonds to enable energy dissipation for selective damping and the necessity for strong bonds to ensure reliable adhesion.

Herein, a Janus adhesive hydrogel was prepared by synergizing natural sedimentation-assisted fabrication with gelation-limited sedimentation, which effectively overcame the aforementioned challenges. The hydrogel achieves adhesion with selective frequency damping by detailed designing the energy dissipating bonding and the adhesion bonding separately. The introduction of electron-conductive particles into the hydrogel improves its dielectric properties, enhances charge transfer, and densifies the electric field, resulting in high-fidelity bioelectrical signal transmission. As a Janus adhesive hydrogel, it exhibits an asymmetric adhesion difference of up to 537 times. By modulating energy dissipation, our hydrogel is capable of selective respiration noise damping and features a damping efficiency in the respiratory frequency range 60 times that in the non-respiratory range. The hydrogel we produced also demonstrated exceptional electrical endurance, enabling 10000-cycle charge injection/ejection during long-term bioelectronic interfacing. Furthermore, we utilized the hydrogel for clinical trials, such as diagnosing otitis media with greater sensitivity than invasive probes and monitoring obstructive sleep apnea (OSA) through polysomnography (PSG).

Results

The design principle and mechanism of JAH

Janus materials are a unique type of functional materials that integrate different compositions and functions, with clear spatial partitioning characteristics. As shown in Fig. 1a, we fabricated a Janus adhesive

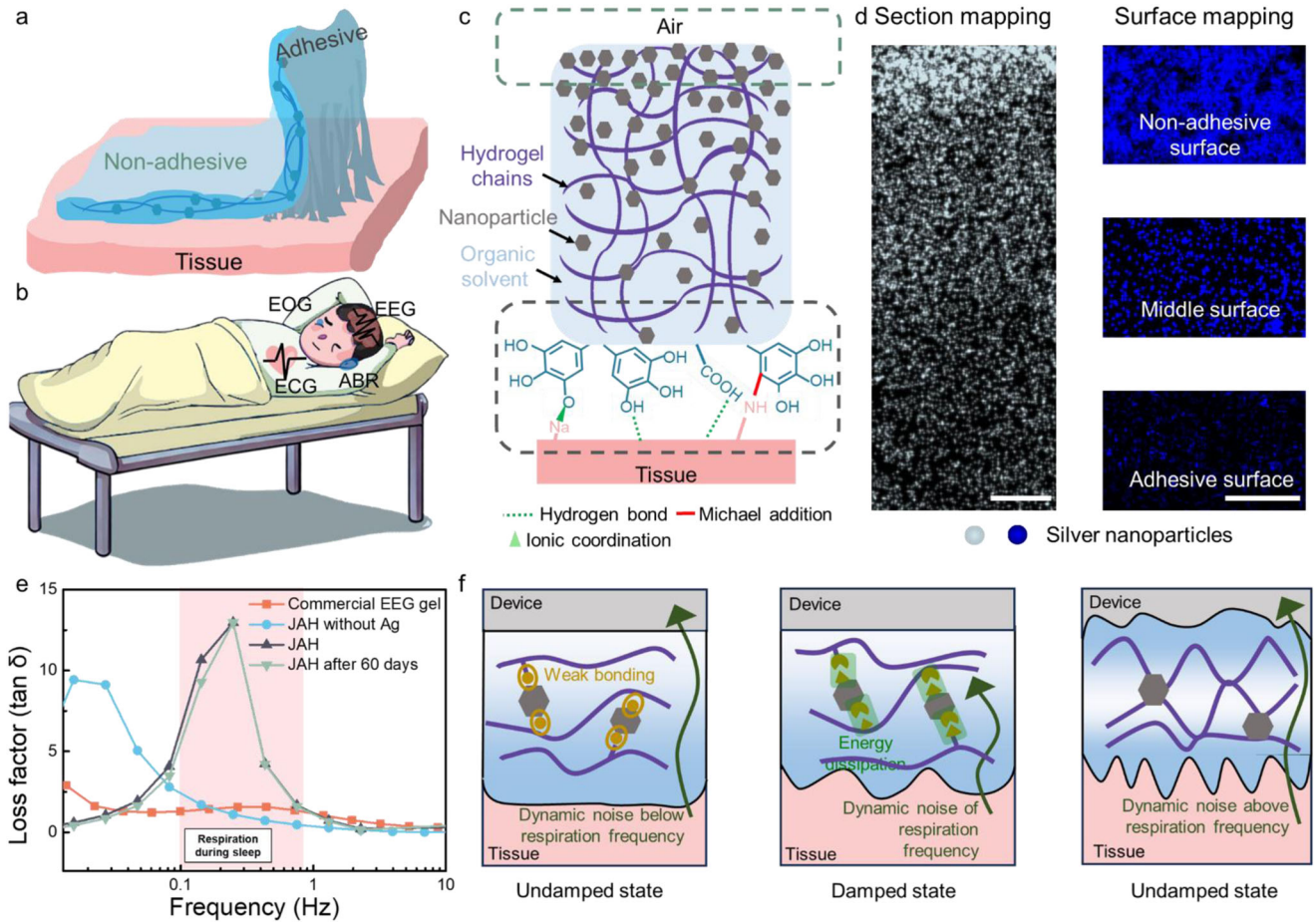

Fig. 1 | The design principle and characterization of JAH. a The asymmetric adhesion of JAH. **b** The clinical practice by JAH. **c** The mechanism of asymmetric adhesion. **d** The section silver element mapping image (scale bar: 500 μm) and surface silver element mapping (scale bar: 100 μm) of JAH. Four independent experiments of each type have been done and produced consistent results. **e** Loss factor of the JAH, JAH without Ag, JAH after 60 days, and commercial EEG gel versus frequency. **f** The damping mechanism of JAH is achieved through energy dissipation resulting from weak bonding.

hydrogel (JAH) with asymmetric adhesion. The adhesive surface can achieve reliable adhesion (> 20 kPa) to the tissue. JAH was used to monitor bioelectrical signals, including electrocardiogram (ECG), electrooculogram (EOG), electroencephalogram (EEG), and auditory brainstem response (ABR) signals (Fig. 1b).

We selected acrylamide for the preparation of hydrogels, introduced ionic conductivity through the addition of sodium chloride, and employed a solvent consisting of ethylene glycol and water to enhance the water retention properties of the JAH. In addition, we integrated silver nanoparticles to enhance the electrical properties of the hydrogels (Supplementary Fig. 1), such as improving dielectric properties, enhancing charge transfer, and densifying the electric field, which will be elaborated on later, along with facilitating bonding for damping purposes. During the gelation process of the JAH, we achieved a Janus structure by synergizing three processes: the natural sedimentation of silver nanoparticles induced by gravity, the inhibition of silver nanoparticle sedimentation by free radicals through coordination, and the rapid depletion of free radicals due to the Trommsdorff-Norrish effect during the polymer chain growth, resulting in the re-sedimentation of the silver nanoparticles[21]. This led to an asymmetric gradient distribution of silver nanoparticles within the Janus hydrogel.

As shown in Fig. 1c, the JAH's free catechol groups enable the formation of Michael addition and hydrogen bonding at the interface of JAH and skin[22]. These mechanisms work synergistically with ionic coordination to provide reliable tissue adhesion. Simultaneously, as the silver nanoparticles are asymmetrically distributed within the JAH, the opposite surface of the JAH cannot form an effective adhesive mechanism due to the significant aggregation of silver particles.

SEM section element mapping of JAH is presented in Fig. 1d, revealing an asymmetric and gradient distribution of silver nanoparticles. The surface element mapping of JAH was also performed, confirming the difference in the distribution of silver nanoparticles at different locations. Optical images of the bottom and top of the JAH also show their very different silver particle distributions (Supplementary Fig. 2).

To investigate the selective damping property of JAH, dynamic mechanical analysis was conducted by frequency sweep with JAH without silver nanoparticles, JAH after 60 days, and commercial EEG gel (Fig. 1e and Supplementary Fig. 3). The results indicate that JAH maintains a high tan δ value (loss factor for dynamic noise) in the respiratory frequency range (0.1–1 Hz), and its selective damping performance[9]. The JAH's absorbed energy per volume is characterized at the respiratory frequency range to investigate its energy absorption capability, the results also indicate its damping characteristics at respiration-related frequencies (Supplementary Fig. 4). Besides, the damping performance remains stable even after 60 days due to JAH's excellent water retention resulting from the hydrogen bond construction between water and ethylene glycol (Supplementary Figs. 5, 6)[23]. In addition to the damping properties, which have been demonstrated to remain stable, the remaining JAH properties have also been shown to remain stable over a 60-day period (Supplementary Table 1). Compared to the adhesive surface, the non-adhesive surface of JAH has better elasticity, suggesting that the incorporation of silver nanoparticles introduces more reversible bonding and thus the non-adhesive surface with more silver nanoparticles has better elasticity (Supplementary Fig. 7). Furthermore, the loss factor results for the adhesive and non-adhesive layers of JAH are found to be disparate (Supplementary Fig. 8a), the effective damping frequency of the non-adhesive surface is greater than the opposite surface. In addition, the utilization of an adhesive layer as the upper surface in comparison to the employment of a non-adhesive layer has a negligible impact on the loss factor (Supplementary Fig. 8b).

As shown in Fig. 1f, the key mechanism of JAH we hypothesize for selective damping is based on the energy dissipation of the weak bonding. External devices may experience bioelectrical signal distortion when dynamic noise with a frequency lower than respiration reaches JAH. This is because the transmission of dynamic noise, which is too weak to break the bonding, can cause such distortion. When the dynamic noise caused by respiration reaches the JAH, the weak bonding within the JAH is interrupted due to the absorption of the noise's energy. This results in energy dissipation, which absorbs the noise within the range of respiration frequency and prevents the distortion of the bioelectric signal. However, if the frequency of the dynamic noise is higher than that of the respiration, the energy of the noise is greater than the energy that can be dissipated by weak bonding, causing the damping to fail. Consequently, the polymer chains and silver nanoparticles undergo a rearrangement, resulting in a reduction of the loss modulus and the introduction of dynamic noise that distorts the bioelectrical signal (Supplementary Fig. 9). In comparison to the hydrogel damper of Park et al., JAH achieves its damping properties without the need for an external heater[9]. The selective damping of dynamic noise is solely achieved through the internal bonding of the JAH itself. This non-temperature-dependent damping property not only simplifies the device's complexity but also prevents water loss in the hydrogel caused by heating.

In summary, the introduction of silver nanoparticles results in our hydrogel acquiring asymmetric adhesion with selective frequency damping properties.

The Janus structure formation and Janus adhesion of JAH

To analyze the process of Janus structure formation in JAH, we determined the gelation time of JAH using solid-liquid balance (SLB) values. The hydrogel is considered fully gelled when the SLB value drops below 0.5 during the gelation process[24]. As shown in Fig. 2a, the gelation time of JAH is about 20 min after the initiator is added into JAH's pre-solution. Then, dynamical instability is used to differentiate between the various stages of Janus structure formation during the gelation process (Fig. 2b). The JAH is divided into top, middle, and bottom sections. The dynamical instability values of all three sections remain constant after 20 min of adding the initiator, which is consistent with the gelation time results characterized by SLB.

Based on the changes in dynamical instability values of its different sections at different times, the gelation process of JAH was divided into five stages. As shown in Fig. 2c, in stage (i), the silver nanoparticles undergo gravity settlement in all three sections of JAH, resulting in an increase in their dynamical instability; in stage (ii), due to the gelation process of JAH resulting in higher viscosity and the silver nanoparticles aggregate and settle most at the bottom of the JAH. As a result, the bottom of the JAH reaches the equilibrium of gravity settlement first, and its dynamical instability no longer changes; in stage (iii), based on the free radical polymerization mechanism, k_d is significantly greater than k_i, resulting in a large number of free radicals produced by the initiator. These free radicals then coordinate with the silver nanoparticles, maintaining dynamical instability at the middle and top of the JAH[25]; in stage (iv), due to the Trommsdorff-Norrish effect, free radicals are rapidly consumed for polymer chain growth. As a result, silver nanoparticles in the middle and bottom sections of the JAH continue to settle at this time; in stage (v), the gelation process of JAH has been completed and the dynamical instability of each section is no longer affected. We investigated the gelation mechanism of JAH and used Fourier Transform infrared spectroscopy (FTIR) to characterize the pre-solution of JAH and the adhesive and non-adhesive surfaces of JAH. After gelation, the FTIR results of the adhesive and non-adhesive surfaces of JAH remained consistent, indicating that the distribution of silver nanoparticles did not affect the molecular structure of JAH (Supplementary Fig. 10). Compared with the pre-solution of JAH, the absence of the characteristic C=C peak (1630 cm^{-1}) for the JAH indicated the complete polymerization of acrylamide monomers[26]. Furthermore, the sedimentation models for the silver particles have been established, and the requisite mathematical calculations have been

https://doi.org/10.1038/s41467-024-52833-1

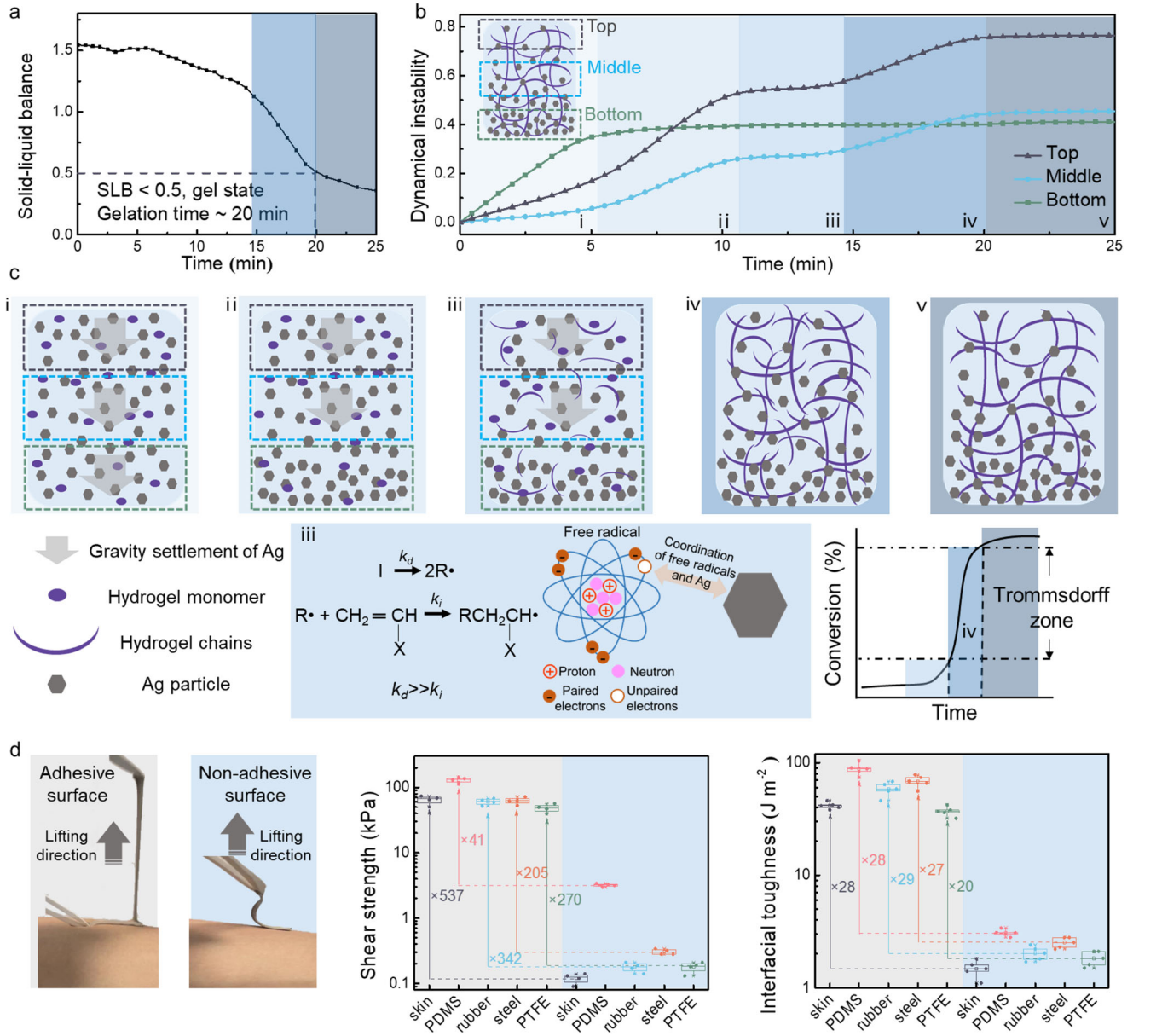

Fig. 2 | The Janus structure formation and Janus adhesion of JAH. a Solid–liquid balance of JAH during gelling. **b** Dynamical instability of different sections of JAH during gelling. **c** The JAH gelation process analysis is based on the stages outlined in (**b**). **d** Adhesion ratios on various substrates between adhesive surface and non-adhesive surface of JAH, $n = 4$ independent samples for each substrate, data represent mean ± standard deviation, the box represents the 25%–75% confidence interval, the square represents the mean, the error bars represent the standard deviation, and the horizontal line in the box represents the median, the symbols are the values obtained for each test.

performed (Supplementary Fig. 11). The modeling and computational results also indicate that during the gelation process of JAH, silver nanoparticles undergo sedimentation and thus form a gradient distribution.

Due to the Janus structure formed during gelation, JAH displays asymmetric adhesion (Supplementary Movie 1). We have characterized the asymmetric adhesion of JAH by peel adhesion (Supplementary Fig. 12) and shear adhesion (Supplementary Fig. 13) tests. As shown in Fig. 2d, the photographs demonstrate that the JAH's adhesive surface adheres well to the skin and that it also exhibits good stretching when peeled off. In contrast, the non-adhesive surface shows minimal adhesion. JAH's adhesive and non-adhesive surfaces exhibit significant differences in adhesion on various substrates. The ratios in shear adhesion are 537, 41, 342, 205, and 270 times on skin, PDMS, rubber, steel, and PTFE, respectively. The differences in peel adhesion are 28, 28, 29, 27, and 20 times on skin, PDMS, rubber, steel, and PTFE, respectively.

Electrical performance of JAH

The electrical properties of hydrogels, which are used as bioelectronic interfaces, are crucial for the transmission of bioelectrical signals. As shown in Fig. 3a, the results of the cyclic voltammetry (CV) test indicate that JAH has a higher current density than commercial EEG gel and maintains excellent CV cycling performance. Furthermore, the CV results of JAH are closer to the ideal CV results without distortion (Fig. 3b), which indicates a reversible electrochemical reaction. In these cases, the electroactive hydrogels undergo oxidation and reduction processes with minimal energy loss, indicating efficient electron transfer. Figure 3c shows the results of electrochemical Bode impedance spectroscopy (EIS), which indicate that JAH has very low impedance (< 50 Ω) at

https://doi.org/10.1038/s41467-024-52833-1

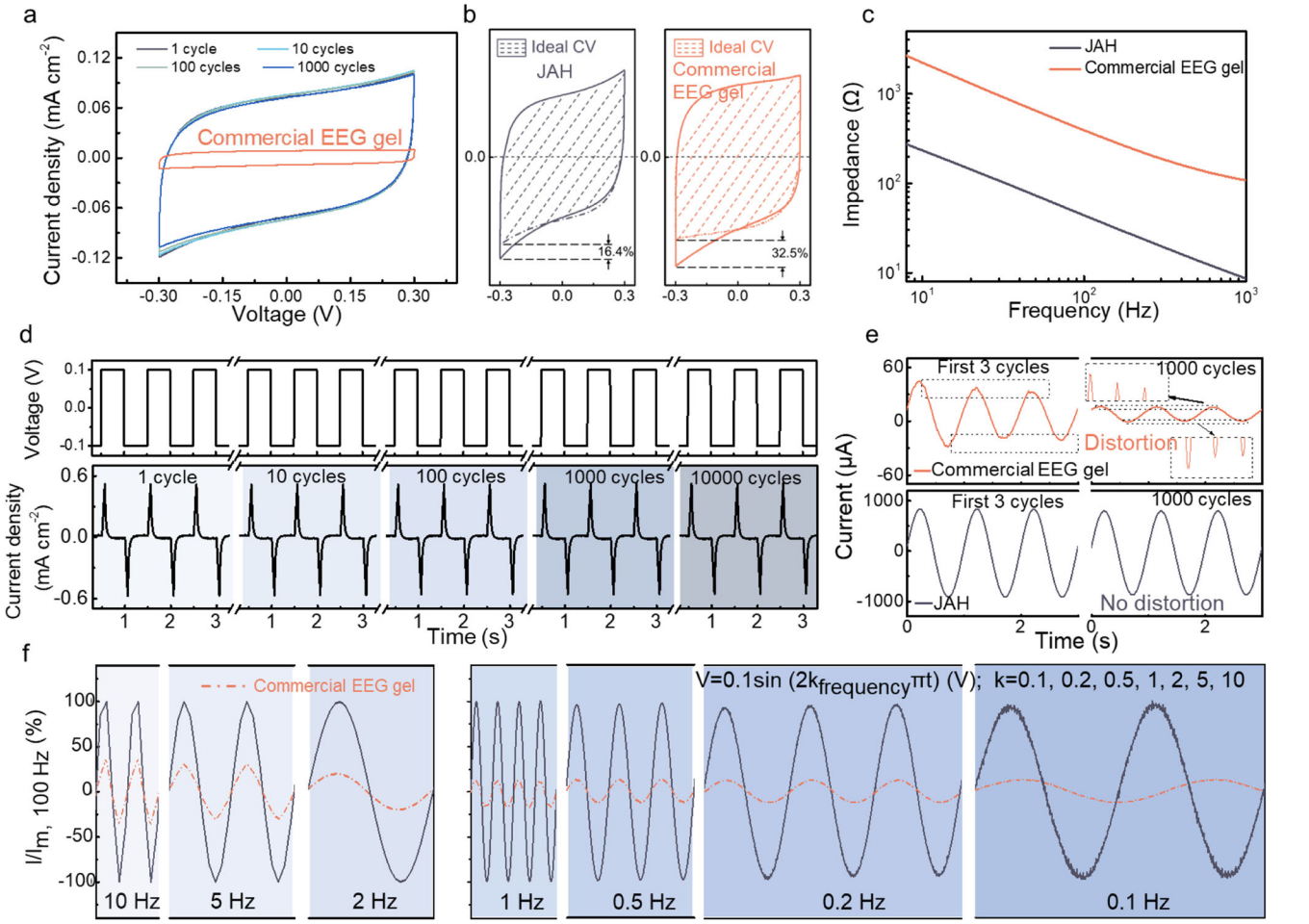

Fig. 3 | Electrical characterizations of JAH. a CV curve of commercial EEG gel and JAH with up to 1000 cycles. **b** Comparison of the deviation of JAH and commercial EEG gel with their ideal CV curves. **c** Impedance comparison between commercial EEG gel and JAH in different directions. **d** Charge injection curves of JAH with biphasic pulses of ± 0.1 V for 10000 cycles. **e** Current vs. time curves of JAH and commercial EEG gel upon sinusoidal AC voltage (amplitude 1 V, frequency 1 Hz). **f** Normalized current vs. time curves of JAH and commercial EEG gel upon sinusoidal AC voltage. For comparison, the currents were normalized to the maximum current value upon the AC voltage of 100 Hz.

physiologically relevant frequencies (100–1000 Hz). In comparison to recently reported studies, the JAH demonstrates advanced impedance performance at physiologically relevant frequencies (Supplementary Table 2). The non-adhesive surface exhibits a lower impedance due to the deposition of silver nanoparticles, in comparison to the adhesive surface (Supplementary Fig. 14). This demonstrates the effect of the sedimentation of silver nanoparticles on the electrical performance of the JAH material. The Bode impedance (Z) is expressed as electrical conduction in the thickness direction (T) of a rectangular body with cross-section dimensions (length L, width W) and thickness T. We normalized the Bode impedance, the volume impedance (Supplementary Fig. 15a) was normalized by Z^*L^*W / T; contact impedance (Supplementary Fig. 15b) was normalized by Z^*L^*W; sheet impedance (Supplementary Fig. 15c) was normalized by Z^*W / T. Furthermore, the phase shift of JAH remains relatively constant within a broad frequency range, in accordance with the expected characteristics of a resistor (0° phase shift) in contrast to the ideal capacitor (90° phase shift) (Supplementary Fig. 16).

Furthermore, when using biphasic pulses of ± 0.1 V, the JAH demonstrates a stable electrical performance even after 10,000 charging and discharging cycles (Fig. 3d). This is due to the improved conductivity and electrochemical stability of the Janus structure. When a sinusoidal signal with a frequency of 1 Hz and an amplitude of 0.1 V is inputted, the JAH exhibits no signal degradation or distortion during long loops, in comparison to the commercial EEG gel (Fig. 3e)[27]. Furthermore, following 1000 cycles, the magnitude of the current observed with JAH increases substantially, from 18.9 times greater than that of the commercial EEG gel to 53.1 times. In comparison to commercial EEG gel, the relative reduction rates of JAH are insignificant, which suggests that JAH is a reliable method for transmitting electrical stimulations (Supplementary Fig. 17). These underscore JAH's remarkable durability and efficiency in electrical performance over extended use. We also characterized the performance of the JAH when subjected to sinusoidal electrical signal inputs of different frequencies (Fig. 3f). As the frequency decreased from 10 Hz to 0.1 Hz, the current measured using the commercial EEG gel experienced a significant reduction, plummeting to merely 10% of its initial value. Furthermore, the commercial EEG gel exhibited a pronounced deviation from sinusoidal current waveforms, particularly at lower alternating current (AC) frequencies. In contrast, the current waveforms obtained through JAH closely mirrored the standard sine wave across all tested frequencies, showcasing JAH's reliable performance as a bioelectronic interface. This demonstrates JAH's capacity for flawless electrical signal transmission, maintaining high-quality signal integrity under varying conditions.

The reasons for JAH's excellent electrical performance have been analyzed[28]. The electrical performance of JAH can be enhanced in three ways (Supplementary Fig. 18):

(1) As demonstrated by the dielectric constant, the silver nanoparticles enhance the dielectric property. According to the double

https://doi.org/10.1038/s41467-024-52833-1

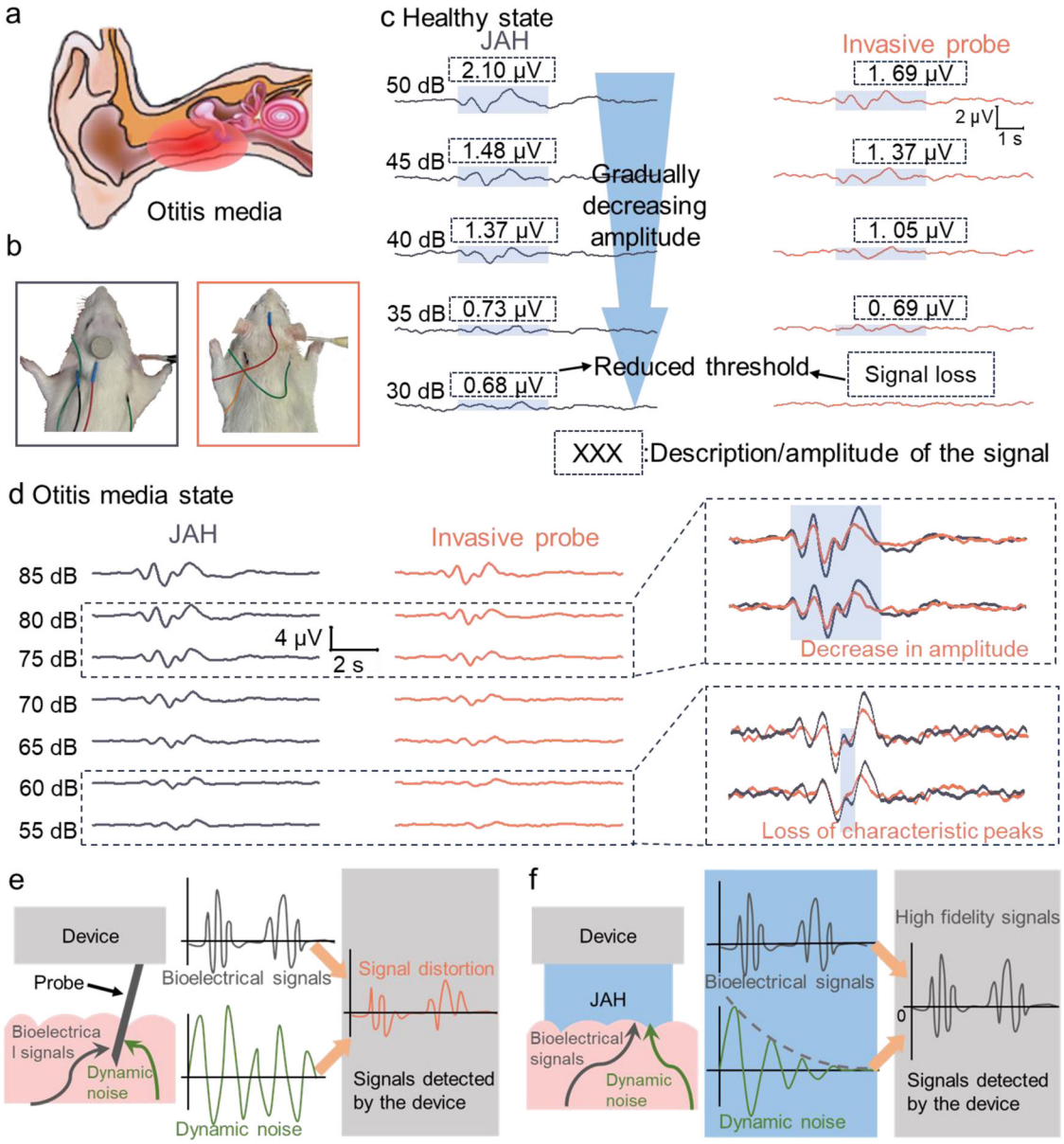

Fig. 4 | Otitis media diagnosis by JAH. a Otitis media sites. **b** Diagnosis of otitis media by JAH (gray frame) and invasive probe (orange frame). **c** Auditory brainstem response (ABR) signals from healthy rats by JAH and invasive probe. **d** ABR signals from rats with otitis media by JAH and invasive probe. **e**, **f** The comparison of the enhancement mechanism of signal quality through damping characteristics of JAH with that of invasive probes.

layer theory, this increased property can result in a more uniform distribution of ions;

(2) Macroscopically, the improvement in dielectric property leads to an extension of the Debye length (the calculation of the Debye length is elaborated upon in the graphical notes, where the formula and its components are detailed comprehensively). Moreover, commercial EEG gel exhibits a layer of opposite charges and a rapidly decaying concentration attributable to the electrical double layer (Supplementary Fig. 18a). Conversely, silver nanoparticles promote a more dispersed charge distribution (Supplementary Fig. 18b). This dispersion necessitates an increased Debye length to accommodate charge depletion, given that the spatial extent of the diffuse double layer and the Debye length are comparable. Such an arrangement enhances double-layer regions and salt solubilization, thereby facilitating improved charge transfer;

(3) Microscopically, when subjected to an electric field, the conductive silver nanoparticles become polarized in a direction opposite to that of the field. This polarization results in the adsorption of a layer of counterions around the nanoparticles, leading to a localized intensification of the electric field in their vicinity. Consequently, this densification of the electric field around the silver nanoparticles enhances the efficiency of charge transfer.

The reliable electrical performances of JAH, as discussed, fulfill the necessary prerequisites for its application in bioelectronic interfaces.

Applications for the diagnosis of otitis media

Based on these characteristics, we applied JAH as a bioelectronic interface. As shown in Fig. 4a, otitis media is an inflammation of the middle ear that can cause ear pain, difficulty hearing, fever, fluid drainage, and irritability in children. Diagnosing otitis media is important not only for addressing immediate discomfort and potential hearing issues but also for preventing long-term health problems and ensuring overall well-being.

During the diagnosis and study of otitis media, the auditory brainstem response (ABR) signal is typically detected (Supplementary Fig. 19). Invasive methods (such as metal probes penetrating

subcutaneously to the skull, Supplementary Fig. 20) with high sensitivity properties are commonly used to improve the accuracy of the signals (Fig. 4b), they can be used to detect signals on the nanovolt scale. In contrast, utilizing JAH as a non-invasive interface (adhering directly to the scalp without piercing the tissue) enables the attainment of superior detection sensitivity compared to that of invasive electrodes. Prior to applying JAH to bioelectrical experiments, we conducted tests to assess its impact on cell viability (Supplementary Fig. 21) and skin inflammation (Supplementary Fig. 22). After 24 h, the cell survival rate was 94.27%. Furthermore, there was no inflammatory response observed in the tissue after the application of JAH.

Firstly, the performance of JAH's high-sensitivity bioelectricity detection was validated in healthy state rats (Fig. 4c). As the sound input's decibel level decreases, the amplitude of the ABR signals obtained by both the JAH and the invasive probe decreases. However, at each decibel level, the JAH's ABR signals have a greater amplitude than those of the invasive probe. The factors that can affect the threshold include external noise, electrode quality, and external currents. As the testing is conducted in a shielded room, the impact of external currents can be considered to be insignificant. The quality of the electrode and the presence of external noise have the potential to influence the outcome of the test, particularly in terms of the amplitude of the recorded waveform. The presence of suboptimal electrodes and considerable external noise can result in the generation of weak and distorted signals, which may lead to an erroneously elevated threshold. It is worth noting that JAH has a detection threshold as low as 25 dB, whereas invasive probes require a threshold of 35 dB (Supplementary Fig. 23). The analysis of the signal-to-noise ratio (SNR) results also demonstrated that JAH exhibited superior ABR signal detection performance compared to the invasive probe (Supplementary Fig. 24).

After validating the high bioelectrical detection sensitivity of the JAH in healthy state rats, we further tested its ability to detect otitis media ABR signals (Fig. 4d). When rats suffer from otitis media, their hearing loss is significant. An invasive probe can only detect the ABR signal produced by rats in response to a sound of 45 dB. However, the JAH was still able to detect ABR signals in rats with otitis media, the detection threshold was as low as 35 dB (Supplementary Fig. 25). Compared to the use of JAH, it is important to note that when rats experience otitis media, the amplitude of ABR signals obtained with invasive probes is reduced and there is also a significant loss of the characteristic peaks of the ABR signals. It is suggested that the invasive probe is unable to dampen the respiratory noise of the rats, while the JAH can avoid the loss of characteristic peaks due to its excellent damping performance in the respiratory frequency range.

When the frequency of the sound used for stimulation varies, the amplitude of the ABR signals obtained by the JAH is greater compared to invasive probes (Supplementary Fig. 26), and the detection threshold of the ABR signals obtained by the JAH is lower (Supplementary Fig. 27), regardless of the health status of the rats, whether healthy or with otitis media. As shown in Fig. 4e, motion artefacts generated by dynamic noise (respiration) are superimposed on the bioelectric signal, thereby leading to signal distortion. The damping properties of the JAH enable the filtering of this dynamic noise (Fig. 4f), thus allowing the external device to obtain a high-fidelity bioelectric signal.

In conclusion, the bioelectrical detection capability of JAH has been validated for high performance.

Applications for clinical sleep monitoring

It is estimated that approximately 1 billion individuals between the ages of 30 and 69 suffer from obstructive sleep apnea (OSA), which is the most prevalent form of sleep-disordered breathing, and 90% of OSA cases go undiagnosed[29]. Sleep monitoring provides valuable insights into one's sleep habits, which are essential for the accurate diagnosis, classification, and management of OSA[30]. Therefore, sleep monitoring is essential for maintaining good physical and mental health, optimizing performance, and improving overall quality of life. As the gold standard of sleep monitoring, polysomnography (PSG) can effectively provide sleep information by detecting signals from electroencephalograms (EEGs), electrooculograms (EOGs), and electrocardiograms (ECGs). The feasibility and superiority of JAH for clinical PSG were validated (Fig. 5a).

In clinical practice, the conductive paste typically leaves irreversible residues on the PSG electrodes due to its isotropic adhesion (Fig. 5a and Supplementary Fig. 28), this can affect the accuracy of bioelectrical signal detection. These PSG electrodes tend to be expensive, resulting in a non-negligible economic loss. However, as JAH exhibits asymmetric adhesion, connecting the non-adhesive surface to the PSG electrodes and the adhesive surface to the human body can effectively solve the residual problem while ensuring the quality of the bioelectric signal acquisition (Fig. 5a). This approach can significantly improve the durability of the PSG electrodes.

As shown in Fig. 5b, during clinical PSG monitoring, the JAH is positioned to monitor ECG, EEG, and EOG signals. When detecting bioelectrical signals, the interface between electrode and device can be depicted as a parallel circuit of the leakage resistance (R_e) and electrical double-layer capacitance (C_e), and the interfacial impedance ($Z_{interface}$) can be calculated from $Z_{interface} = (1/R_e + sC_e)^{-1}$ where s represents the frequency of the electrophysiological signal. As shown in Fig. 5c, the residual gel, which is challenging to remove, contracts in volume over time due to water loss, resulting in gaps at the interface with the device, which reduces the C_e. Furthermore, the cracks created within the gel impede the transport of ions, thus increasing the R_e. In contrast, JAH is designed to avoid the formation of residues due to its asymmetric adhesion, besides, it is formulated to prevent problems associated with water loss due to its long-term stability, which is achieved through the introduction of organic solvents.

We analyzed the ECG signals obtained from commercial conductive gel and JAH. After the Fourier transform, it is evident that JAH has significant dynamic noise damping in the range of 0.1–1 Hz, demonstrating its effectiveness in selective frequency damping performance (Fig. 5d). A comparative analysis of commercial EEG gel and JAH indicates that the JAH exhibits superior performance in both root mean square (RMS) noise and signal amplitude metrics (Supplementary Table 3).

JAH can be utilized for PSG monitoring to capture characteristic signals representing different sleep stages (Fig. 5e), including the α rhythm during the awake stage, saw-tooth waves during rapid eye movement (REM) sleep, slow eye movements in non-rapid eye movement 1 (N1) sleep, spindle waves and K-complexes in non-rapid eye movement 2 (N2) sleep, and δ waves in non-rapid eye movement 3 (N3) sleep. Moreover, JAH can also record ECG signals during sleep. The JAH material was employed for the acquisition of EEG signals at the F4, C4, and O2 positions of the brain, while a commercial EEG gel was utilized for EEG acquisition at the F3, C3, and O1 positions, which were located in a symmetrical manner relative to the JAH positions (Supplementary Fig. 29a). However, the signals from the commercial EEG gel exhibited a shortened duration of characteristic waveforms, signal loss, and an absence of characteristic waveforms, which may compromise the precision of PSG results (Supplementary Fig. 29b). Therefore, the utilization of JAH as a PSG monitoring material facilitates a detailed examination of sleep structure, the prompt identification of sleep disorders and the formulation of personalized treatment plans. Furthermore, it reduces the incidence of misdiagnosis and underdiagnosis. Clinicians leverage the signals acquired by JAH to classify the patient's sleep stages (Supplementary Fig. 30) and calculate the apnea-hypopnea index (AHI) (Supplementary Table 4). Ultimately, it can lead to the diagnosis of obstructive sleep apnea (OSA) (Supplementary Table 5).

In conclusion, the validity and superiority of JAH in clinical PSG monitoring are confirmed.

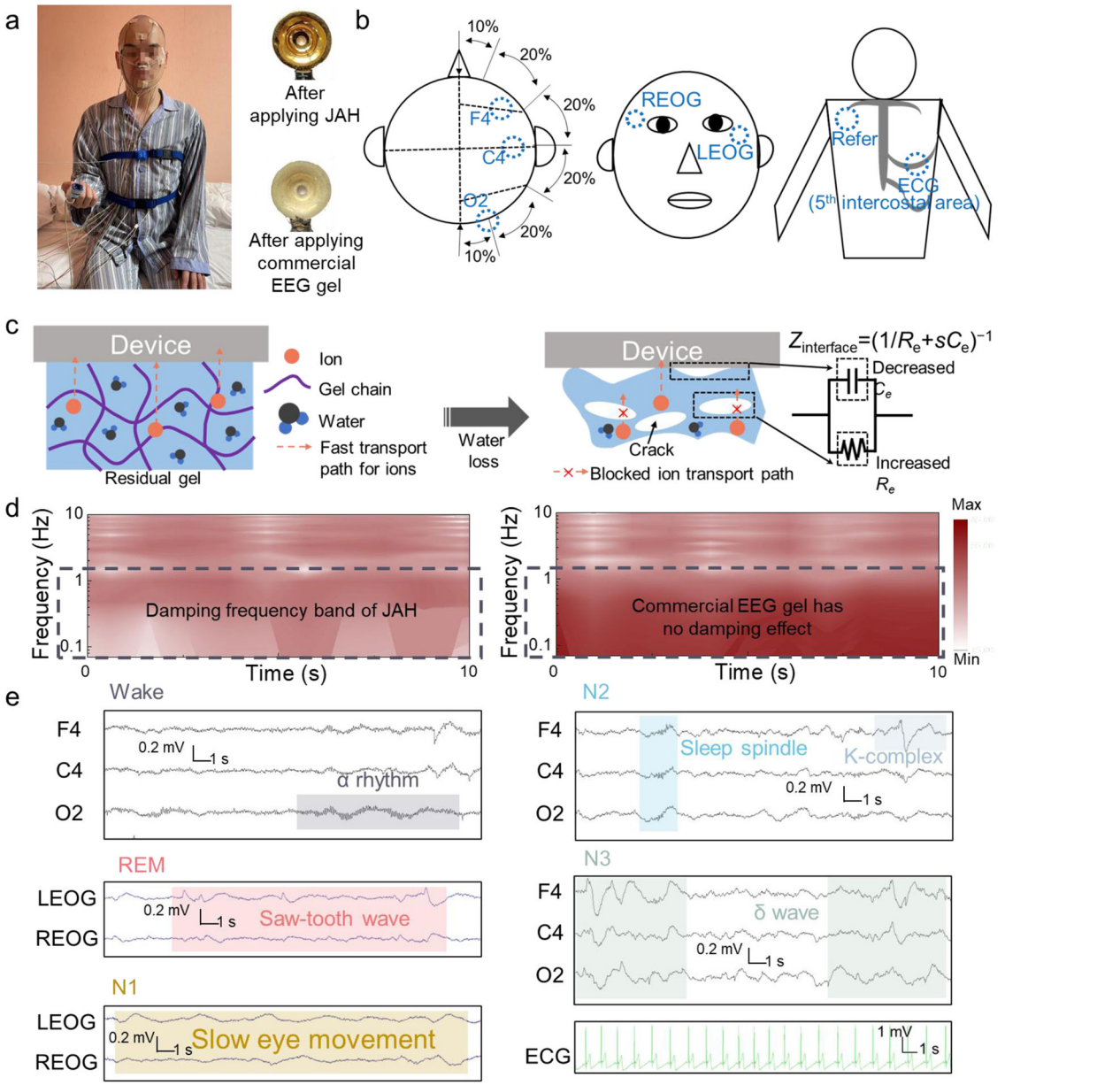

Fig. 5 | Clinical sleep monitoring by JAH. a Clinical sleep monitoring and the difference in device electrodes after using JAH and commercial EEG gel. **b** The positions of JAH for EEG, EOG, and ECG during clinical sleep monitoring. **c** Effect of residual gel on bioelectrical signals. **d** Damping effect of JAH on dynamic noise in the frequency range 0.1–1 Hz. **e** Raw EEG, EOG, and ECG data measured from the polysomnography (PSG) system (F4, C4, O2. LEO, REOG) by JAH, capturing the characteristic signals of the five sleep stages (awake, N1, N2, N3, and REM).

Discussion

This study introduces a hydrogel exhibiting selective frequency-damping properties and asymmetric adhesion for bioelectronic interfaces. The hydrogel effectively dampens dynamic noise within the breathing frequency range while maintaining exceptional and stable electrical properties, low impedance, and biocompatibility. Detailed analysis is provided on the formation process of the asymmetric structure and the optimization mechanism of the hydrogel's electrical properties. Serving as a non-invasive approach, our hydrogel demonstrates heightened sensitivity compared to invasive electrodes for detecting bioelectrical signals, attributed to its damping capabilities against dynamic noise. Moreover, we have substantiated the efficacy of our hydrogel in clinical PSG monitoring, showcasing its utility in aiding clinicians with OSA diagnosis. Based on our research, we believe there is a need for the development of damping hydrogels with enhanced properties, the establishment of a robust integration between hydrogels and electronics, and the introduction of advanced fabrication methodologies for damping hydrogel bioelectronics.

Methods

Materials

Acrylamide, tannic acid, N, N′-methylene-bis(acrylamide) (MBA), ammonium persulfate (APS), and sodium chloride were purchased from Sigma-Aldrich. Ethylene glycol and silver nanoparticles were purchased from Aladdin. All the chemicals were used as received without further purification. The commercial EEG gel (Ten 20, Weaver and Company, USA) was purchased from Jingdong JD.com, Inc).

Preparation of JAH

(1) Mix 4 ml deionized water and 5 ml ethylene glycol with the monomer of 1.5 g acrylamide, 0.02 g tannic acid, and 1 g sodium chloride. (2) Add 0.005 g MBA crosslinking agent and 2 g silver nanoparticles. (3)

Stir the solution for 20 min, and then defoam the pre-solution by ultrasonic. (4) Add a mixed solution of 0.1 g APS and 1 mL deionized water. (5) Pour the pre-solution into a 2 mm thickness polytetrafluoroethylene (PTFE) mold for 20 min heating under 45 °C, then JAH is obtained. Supplementary Table 6 shows the relationship between mold thickness and temperature selection for achieving asymmetric adhesion.

Electrical performance characterization

For characterizing the impedance performance of JAH, an electrochemical workstation (Biologic SAS, VSP-300, France) was used, Supplementary Fig. 31 shows the geometrical and technical properties of this characterization. When characterized the electrical stability, the JAH received the signal from an electrical signal generator through a series connection.

Otitis media diagnosis and clinical PSG monitoring

The ABR signals were recorded by RZ6 (Tucker-Davis Technologies, USA), a pack of three 12 mm long needles (29 gauge) electrodes (112-812-48TP, Chalgren Enterprises, Inc., USA) was utilized (Supplementary Fig. 32), each equipped with a 30 cm lead wire terminating in a 1.5 mm shrouded female plug. The ABR was recorded using three subdermal electrodes. The recording electrode was inserted at the vertex of the rat's skull (Sprague Dawley rat, 8–10 weeks, female), while the reference and grounding electrodes were positioned separately on the mastoid regions on both sides. Supplementary Fig. 19 shows the test method for ABR signals. The Institutional Animal Care and Use Committee (IACUC) of Shanghai Jiaotong University School of Medicine, affiliated with Shanghai Sixth People's Hospital, approved the animal experimental research project (Animal Welfare Ethics acceptance number No: DWLL2024-0557; Animal Experiment Registration number No: DWSY2023-0087).

The sleep was monitored by a PSG system (Premium Alice 6 LDxS PSG Sleep System, Philips, Netherlands), and the data underwent processing via the PSG System's affiliated software. (Sleepware G3, Philips, Netherlands). The cutoff frequencies of the bandpass filter recommended by the American Academy of Sleeping Medicine guidelines were 0.3–5 Hz for EEG and EOG and 0.3–70 Hz for ECG. The JAH utilized in the examination was 2 mm in thickness.

For the clinical study with sleep disorder patients, informed consent was received with a signed consent form before the sleep measurement at the Shanghai Key Laboratory of Sleep Disordered Breathing. The study followed the approved protocol from the Ethics Review Board of Shanghai Sixth People's Hospital under Protocol Number 2021-KY-76.

We have confirmed that informed written consent from all participants or next of kin was obtained prior to the research. The application as the bioelectronics was done on the first author and the safety was demonstrated by biocompatibility and skin irritation tests prior to characterization.

Characterization and measurements

The loss factor is characterized by a rheometer (Rheolaser Master, Formulaction, France). The image with super depth of field was captured using a Super Depth of Field Microscope (DVM6, Leica, Germany). Element mapping was measured using a scanning electron microscope (FE-SEM; SU8000, Hitachi, Japan). The storage environment for JAH's long-term stability testing is provided by a constant temperature and humidity chamber (SGDW-100L-60, Sanliang, Japan), which maintains a stable and controlled environment (25 °C, 60% humidity) for the duration of the testing period. The dielectric constant was determined through dielectric impedance spectroscopy (Concept 40*, Novocontrol, Germany). Infrared characterization of the gelation mechanism was performed using a Fourier infrared spectrometer (Nicolet iS50, Thermo Scientific, USA). Adhesion force characterizations were conducted using an electronic universal material testing machine (Model 5969, Instron, USA) equipped with a 10 N load cell and 5 N clamp. Histological results were obtained by applying JAH and commercial EEG gel (Ten 20, Weaver and Company, USA) to the skin of a mouse for 24 h, followed by hematoxylin-eosin staining of the corresponding biological tissues. Cell viability results were obtained by culturing L-929 cells (cells were obtained from the Chinese Academy of Sciences cell bank, Shanghai, China) for 24 h and comparing them with a complete medium containing 10% fetal bovine serum (Zhejiang Tianhang Biotechnology Co., Ltd.) of MEM medium (Hangzhou Ji Nuo Biomedical Technology Co., Ltd.). The multiple light scattering measurements (Turbiscan Tower, Formulaction, France) were used to characterize the dynamical instability, the instrument automatically divided the samples into upper, middle, and lower parts in a uniform manner.

Reporting summary

Further information on research design is available in the Nature Portfolio Reporting Summary linked to this article.

Data availability

All data supporting the findings of this study are available within the article and its Supplementary files. Any additional requests for information can be directed to, and will be fulfilled by, the corresponding authors. Figshare are provided with this paper. Source data are provided in this paper.

References

1. Zhang, B. et al. A three-dimensional liquid diode for soft, integrated permeable electronics. *Nature* **628**, 84–92 (2024).
2. Viana, D. et al. Nanoporous graphene-based thin-film microelectrodes for in vivo high-resolution neural recording and stimulation. *Nat. Nanotechnol.* **19**, 514–523 (2024).
3. Xue, Y., Chen, X., Wang, F., Lin, J. & Liu, J. Mechanically-compliant bioelectronic interfaces through fatigue-resistant conducting polymer hydrogel coating. *Adv. Mater.* **35**, 2304095 (2023).
4. Zhao, Y. et al. A self-healing electrically conductive organogel composite. *Nat. Electron.* **6**, 206–215 (2023).
5. Yin, J., Wang, S., Tat, T. & Chen, J. Motion artefact management for soft bioelectronics. *Nat. Rev. Bioeng.* **2**, 541–558 (2024).
6. Park, B. et al. Materials and structural designs toward motion artifact-free bioelectronics. *Chem. Rev.* **124**, 6148–6197 (2024).
7. Lee, K. et al. Mechano-acoustic sensing of physiological processes and body motions via a soft wireless device placed at the suprasternal notch. *Nat. Biomed. Eng.* **4**, 148–158 (2020).
8. De Luca, C. J., Gilmore, L. D., Kuznetsov, M. & Roy, S. H. Filtering the surface EMG signal: Movement artifact and baseline noise contamination. *J. Biomech.* **43**, 1573–1579 (2010).
9. Park, B. et al. Cuticular pad–inspired selective frequency damper for nearly dynamic noise–free bioelectronics. *Science* **376**, 624–629 (2022).
10. Shin, J. H. et al. Polymeric conductive adhesive-based ultrathin epidermal electrodes for long-term monitoring of electrophysiological signals. *Adv. Mater.* **36**, 2313157 (2024).
11. Pan, L. et al. A compliant ionic adhesive electrode with ultralow bioelectronic impedance. *Adv. Mater.* **32**, 2003723 (2020).
12. Zhao, Y. et al. Supramolecular adhesive hydrogels for tissue engineering applications. *Chem. Rev.* **122**, 5604–5640 (2022).
13. Li, S., Cong, Y. & Fu, J. Tissue adhesive hydrogel bioelectronics. *J. Mater. Chem. B* **9**, 4423–4443 (2021).
14. Luo, J. et al. Topological MXene network enabled mixed ion–electron conductive hydrogel bioelectronics. *ACS Nano* **18**, 4008–4018 (2024).
15. Yuk, H., Wu, J. & Zhao, X. Hydrogel interfaces for merging humans and machines. *Nat. Rev. Mater.* **7**, 935–952 (2022).

16. Deng, J. et al. Electrical bioadhesive interface for bioelectronics. *Nat. Mater.* **20**, 229–236 (2021).
17. Shin, Y. et al. Low-impedance tissue-device interface using homogeneously conductive hydrogels chemically bonded to stretchable bioelectronics. *Sci. Adv.* **10**, eadi7724 (2024).
18. He, Y. et al. A smart adhesive Janus hydrogel for non-invasive cardiac repair and tissue adhesion prevention. *Nat. Commun.* **13**, 7666 (2022).
19. Wang, H. et al. An Integrally formed Janus hydrogel for robust wet-tissue adhesive and anti-postoperative adhesion. *Adv. Mater.* **35**, 2300394 (2023).
20. Xu, Y. et al. Magneto-induced Janus adhesive-tough hydrogels for wearable human motion sensing and enhanced low-grade heat harvesting. *ACS Appl. Mater. Interfaces* **16**, 10556 (2024).
21. Zhao, J. et al. Multiscale structural triboelectric aerogels enabled by self-assembly driven supramolecular winding. *Adv. Funct. Mater.* **34**, 2400476 (2024).
22. Pei, X., Zhang, H., Zhou, Y., Zhou, L. & Fu, J. Stretchable, self-healing and tissue-adhesive zwitterionic hydrogels as strain sensors for wireless monitoring of organ motions. *Mater. Horiz.* **7**, 1872–1882 (2020).
23. Luo, J. et al. A bio-adhesive ion-conducting organohydrogel as a high-performance non-invasive interface for bioelectronics. *Chem. Eng. J.* **427**, 130886 (2022).
24. Luo, J. et al. MXene-enabled self-adaptive hydrogel interface for active electroencephalogram interactions. *ACS Nano* **16**, 19373–19384 (2022).
25. Wang, F., Cui, A., Hu, Z. & Zhang, L. Photogated coordination switching of silver nanoparticles for reversible coloration/discoloration of hydrogel. *Adv. Opt. Mater.* **9**, 2101505 (2021).
26. Ge, G. et al. $Ti_3C_2T_x$ MXene-activated fast gelation of stretchable and self-healing hydrogels: a molecular approach. *ACS Nano* **15**, 2698–2706 (2021).
27. Yao, B. W. et al. Ultrastrong, highly conductive and capacitive hydrogel electrode for electron-ion transduction. *Matter* **5**, 4407–4424 (2022).
28. Guo, X. L. et al. A stable solid polymer electrolyte for lithium metal battery with electronically conductive fillers. *Angew. Chem. Int. Ed.* **62**, e2022175 (2023).
29. Lyons, M. M., Bhatt, N. Y., Pack, A. I. & Magalang, U. J. Global burden of sleep-disordered breathing and its implications. *Respirology* **25**, 690–702 (2020).
30. Kwon, S. et al. At-home wireless sleep monitoring patches for the clinical assessment of sleep quality and sleep apnea. *Sci. Adv.* **9**, eadg9671 (2023).

Acknowledgements

We gratefully acknowledge the financial support by the National Natural Science Foundation of China (No. 82301331), the DHU Distinguished Young Professor Program (LZA2023001), the Fundamental Research Funds for the Central Universities (2232024Y-01), and Graduate Student Innovation Fund of Donghua University (CUSF-DH-D-2022017), and Shanghai Pujiang Program (22PJD050).

Author contributions

J.B.L. and Y.F.J. contributed equally to this work. C.Y.H. and S.K.Y. guided the project. C.Y.H. and J.B.L. conceived the idea and designed the experiment. J.B.L., Y.F.J., B.Y.C., B.Z., K.R.L., Q.H.Z., Y.G.L., and H.Z.W. performed the experiments and measurements. J.W., L.P.L., and H.W. revised the manuscript. J.B.L., Y.F.J., L.P.L., and H.W. participated in the ABR test and PSG monitor. All authors analyzed the experimental data, drew the figures, and prepared the manuscript. All authors discussed the results and reviewed the manuscript.

Competing interests

The authors declare no competing interests.

Additional information

Supplementary information The online version contains supplementary material available at https://doi.org/10.1038/s41467-024-52833-1.

Correspondence and requests for materials should be addressed to Linpeng Li, Hui Wang or Chengyi Hou.

Peer review information *Nature Communications* thanks Tae-il Kim, Wenlong Xu, and the other anonymous reviewer(s) for their contribution to the peer review of this work. A peer review file is available.